A&A 472, 691–698 (2007)
DOI: 10.1051/0004-6361:20077421

Astronomy & Astrophysics

A study of the interaction of CO_2 with water ice

O. Gálvez[1], I. K. Ortega[1], B. Maté[1], M. A. Moreno[1], B. Martín-Llorente[1], V. J. Herrero[1], R. Escribano[1], and P. J. Gutiérrez[2]

[1] Instituto de Estructura de la Materia, CSIC, Serrano 123, 28006 Madrid, Spain
e-mail: rescribano@iem.cfmac.csic.es
[2] Instituto de Astrofísica de Andalucía, CSIC, Aptd. 3004, 18080 Granada, Spain

Received 6 March 2007 / Accepted 4 June 2007

ABSTRACT

Aims. We studied the interaction between CO_2 (guest) and H_2O (host) molecular ices.
Methods. Ices of CO_2 and H_2O are prepared by four different deposition techniques: sequential deposition (amorphous water ice followed by addition of CO_2), co-deposition (both gases added simultaneously), inverse sequential deposition (carbon dioxide ice followed by addition of water) and crystalline sequential deposition (crystalline water ice is prepared first and CO_2 is added afterwards). Samples are deposited at 80 K and are studied by temperature programmed desorption and transmission infrared spectroscopy.
Results. Two slightly different varieties of association of CO_2 and H_2O are revealed from the different spectroscopic properties of the asymmetric stretching band of $^{12}CO_2$ and $^{13}CO_2$. The two varieties are found to co-exist in some of the samples at 80 K, whereas only the so-called internal CO_2 remains after heating at 105 K. At 80 K carbon dioxide is able to adhere to a crystalline water ice surface. Activation energies for the desorption of CO_2 from amorphous ($E_d = 20.7 \pm 2$ kJ mol^{-1}) and crystalline ($E_d = 19.9 \pm 2$ kJ mol^{-1}) water ice are derived from measurements of the sticking of CO_2 as a function of ice temperature.
Conclusions. These findings may have implications for the study of icy bodies of the Solar System.

Key words. molecular data – molecular processes – techniques: spectroscopic – methods: laboratory

1. Introduction

Ices, understood as condensed phases of e.g. H_2O, CO, CO_2, CH_3OH, NH_3, CH_4, etc. are ubiquitous throughout the Universe. Ices can be found in dense and cold regions of the interstellar medium, where stars are initially born (Boogert & Ehrenfreund 2004; Ehrenfreund et al. 2003; Gerakines et al. 2005). In particular, the instruments on board the Infrared Space Observatory (ISO) revealed that H_2O, CO_2 and CH_3OH ices were even dominating grain surfaces in warm regions close to massive protostars (Dartois 2005; Van Dishoeck 2004; Ehrenfreund et al. 1997; and references therein). For Solar System research, ices are, in addition, of clear cosmogonic importance. Comets and Kuiper Belt objects are made up of dusty ices mixtures (see e.g. reviews by Crovisier 2006 and Meech & Svoren 2003). As they are, presumably, the less evolved objects of the Solar System, these bodies preserve information about the conditions under which our planetary system formed. At a closer view, ices are even vital for our own climate. Icy particles in our atmosphere signifi cantly affect atmospheric chemistry (Hung et al. 2003; Baker 1997; Tolbert & Toon 2001).

Ices and ices mixtures have been studied from many different standpoints, with very different techniques. In the astrophysical context, part of the knowledge about their composition, physical state, microstructure, and evolution has been derived by means of spectroscopic studies, mainly in the infrared, comparing observational evidence with results from the laboratory. Some interesting investigations, to mention but a few, are: Bernstein et al. (2005, 2006), Gerakines et al. (2005), Grundy & Schmitt (1998), Moore & Hudson (1993), Moore et al. (2001), Quirico et al. (1996), Satorre et al. (2001), Schmitt et al. (1989), van Broekhuizen et al. (2006), etc. This kind of study has provided the community with an important database on spectroscopic behavior of ices under very different conditions, which have allowed the detection of different ices in various astronomical environments. As an example, among many relevant ones, Sandford & Allamandola (1990) showed that laboratory spectra of CO_2 can be used both to derive column densities of CO_2 condensed in interstellar grains, and to obtain clues on the thermal history of interstellar ices. These results have been widely used as, for example, in the recent detection of CO_2 on Saturn's satellite Iapetus (Buratti et al. 2005).

The ubiquity and importance of ices require steadfast efforts on a complete characterization of their behavior under different physical conditions. In the present investigation, we focus on mixtures of ices of H_2O and CO_2. A study in line with the present one was performed by Ehrenfreund et al. (1999). These authors studied infrared spectra of H_2O, CO_2 and CH_3OH ices mixtures, formed by co-deposition and exposed both to thermal and to UV irradiation processing. The main result from their study was that H_2O, CO_2 and CH_3OH bands can indeed be used to trace the evolution of ice composition in dense interstellar clouds. In the present investigation several deposition methods and different thermal histories will be studied. These various methods could represent different formation mechanisms and/or different evolutionary phases of icy mantles (e.g. Boogert & Ehrenfreund 2004). The evolution, as the temperature increases, of the various structures formed with the different deposition methods, and its implications both from thermophysical and spectroscopic standpoints, are of great importance not only to appropriately analyze and interpret remote spectroscopic data, but also for the modeling of the thermophysical evolution of Solar System minor bodies, among other possible applications.

Besides those already cited, there are a number of papers based on laboratory investigations on the field of the interaction between gases and water ice, using temperature-programmed desorption (TPD) techniques based on mass spectrometry (Viti et al. 2004; Notesco et al. 2003; Hudson & Donn 1991), molecular beam techniques (Andersson et al. 2004), or infrared spectroscopy (Bar-Nun & Laufer 2003), among many others. Two very recent papers deal with systems closely related to that of the present investigation, and will be discussed in greater detail. Collings et al. (2004) have carried out an extensive laboratory survey of astrophysical ices of several molecules, using TPD. They studied the adsorption of these molecules on a bare gold substrate, and also their adsorption on water films previously deposited (subsequently referred to in this article as sequential deposition), and after simultaneous deposition with water (co-deposition). They ranked the systems under study in three categories, according to their volatility or similarity to water. Thus, CO, N_2, O_2 and CH_4 are the most volatile; NH_3, CH_3OH and HCOOH are the least volatile or closest to water; and H_2S, OCS, C_2H_2, SO_2, CH_3CN, and CO_2 are intermediate species. The molecule studied in this work, carbon dioxide, falls therefore into the third type. The findings of Collings et al. are discussed below, in comparison with our present results. On the other hand, Kumi et al. (2006) have presented a thorough study on the guest-host interactions of amorphous solid water (ASW) with CO_2 and N_2O molecules, using Fourier transform infrared spectroscopy (FTIR). Based on spectra taken at their deposition temperature (90 K) and after heating to higher temperatures, they were able to propose a mechanism for the adsorption, binding and transport of these two molecules in ASW films. Again, the results of the present investigation will be compared to those of Kumi et al. in the appropriate sections below.

Our research uses a combination of the two techniques mentioned above, TPD and FTIR, on a variety of experimental conditions. We have studied water/CO_2 systems in an approximate 15/1 ratio. The samples were prepared by four deposition techniques. The behavior of the samples on heating is also investigated. The objective of this research is to throw some more light on the adsorption and diffusion processes that take place between the guest (CO_2) and host (H_2O) molecular ices. We find it particularly interesting that some of our results reproduce closely those of the above mentioned references, but others show different characteristics. Besides, we present new evidence, notably on spectra of co–deposited samples. We have also measured activation energies for the desorption of CO_2 from amorphous and crystalline water ice from spectroscopic experiments.

2. Experimental part

Our experimental set-up shown in Fig. 1 has been described in detail before (Carrasco et al. 2002; Escribano et al. 2003; Maté et al. 2003; Maté et al. 2006). In brief, it consists of a high vacuum cylindrical chamber, evacuated by a turbomolecular pump, in whose interior a sample holder, connected to a liquid nitrogen Dewar, provides the appropriate substrate for the deposition of the systems to be studied. The chamber pressure is monitored between 1000 and 10^{-9} mbar by a combination of a pirani and a penning gauge. In addition, a capacitance manometer (Leybold, Ceravac CTR81) provides absolute pressure readings in the 10^{-2}–10^{-5} mbar range. The background pressure in the chamber is usually smaller than 10^{-8} mbar. The chamber is coupled to a Fourier transform infrared spectrometer Bruker IFS66 through a purged pathway, with KBr windows for the incident and transmitted radiation, which is focused on exit onto a

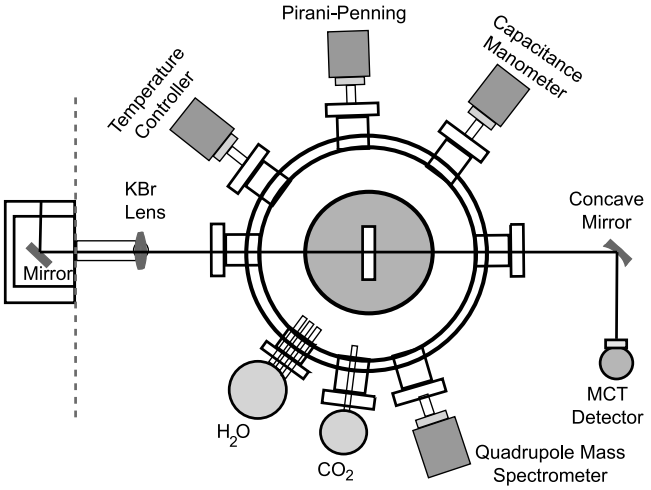

Fig. 1. Scheme of the experimental set-up used for the deposition and study of the ice films.

liquid-N_2 refrigerated MCT detector. In the transmission set-up used in the present experiments, the substrate on which samples are deposited is a Si wafer of about 1 mm thickness. The IR spectrum of this wafer is used as background for ratioing the spectra of the different samples. Spectra are recorded with a nominal resolution of 2 cm^{-1} (corresponding to ~0.5 cm mirror displacement), with 512 co-added scans for each spectrum. A three term Blackman-Harris apodization function is used in all cases. The substrate is mounted on a holder that allows temperature control, with about 1 K accuracy, between 80 and 220 K. Heating is performed using a power transistor (2N3055). Controlled flows of CO_2 and water vapor are introduced into the chamber through needle valves. The chamber has inlets for the insertion of gases, and is coupled by means of a regulation valve to a differentially pumped chamber containing an Inficon, Transpector 2 quadrupole mass spectrometer (QMS), which is used to monitor the vapor composition during the deposition and heating processes. A pressure difference of two orders of magnitude was usually maintained between the deposition and the quadrupole chamber. Typical deposition pressures are always below 10^{-4} mbar.

Films of H_2O/CO_2 ice were prepared in different ways (see below) by vapor deposition on the substrate held at a temperature of ~80 K. Distilled water and 99.998 % purity CO_2 from Air Liquide were used in all experiments. To monitor the thickness and H_2O/CO_2 ratio in each experiment, combined use of spectral data and quadrupole measurements was made, according to the following scheme. For pure water, the film thickness can be easily controlled through the interferences of a normal-incident He-Ne laser (Maté et al. 2003), and for a given thickness value, comparison to literature absorbance data (Léger et al. 1983) allows the estimation of the amount of water deposited on the substrate. Similarly, the observed absorbance of a given sample of pure CO_2, compared to previous measurements (Ehrenfreund et al. 1997), can be used to calibrate the QMS with sufficient accuracy. Then, for any kind of deposition scheme, the quadrupole readings can be used to select the amount of either gas introduced into the chamber. An H_2O:CO_2 value of ~15:1 was chosen for the present investigation. Typical thickness values of 0.3 μm were estimated for the water ice films at each side of the substrate. A sticking efficiency of 1.0 was assumed for both species at 80 K, although in the case of pure CO_2 this value could be slightly lower (Sandford & Allamandola 1990).

The four different deposition procedures employed for the generation of the various types of samples are the following:

- *Sequential deposition*: first the host species, water, is deposited at 80 K as amorphous (ASW), and then CO_2 is added at the same temperature, until the chosen ratio host/guest, is accomplished.
- *Co-deposition*: water and CO_2, are introduced into the chamber simultaneously, at the appropriate ratio, and deposited on the substrate at 80 K.
- *Inverse sequential deposition*: first the desired amount of CO_2 is introduced into the chamber with the substrate at 80 K. At this temperature, crystalline CO_2 is expected to form. Water is then admitted, always keeping the substrate at the same temperature, until the chosen guest/host ratio is reached.
- *Crystalline sequential deposition*: water is first deposited at 80 K. The temperature is then raised up to 165 K and kept there for five minutes to induce crystallization from the amorphous phase. The crystalline water film is subsequently cooled to 80 K, and CO_2 is then admitted until the desired ratio is achieved.

Both TPD and IR absorption measurements were performed on the various ice films. The TPD measurements covered the range 80–190 K, which includes the desorption peaks corresponding to the stronger guest-host interactions. Most of the weakly bound CO_2 was desorbed at nominal temperatures around 90–110 K, but in this temperature interval part of the desorbed CO_2 comes from cold cryostate surfaces apart from the substrate. It is difficult to estimate the contribution of this kind of desorption, which gives rise to an artificial broadening of the peaks, and we have not considered these results here. No more CO_2 is seen to desorb until a temperature above 150 K, and therefore our study deals with the 150–190 K range. A heating ramp of 0.3 K s^{-1} was used for the TPD experiments. Due to some difficulties for the synchronization of the QMS with the heating ramp, there is an uncertainty of approximately 5 K in the absolute temperature scale of the TPD graphs.

Infrared spectra of the four types of film described above were recorded at 80 K, the lowest film temperature, and at 105 K, where some modifications in the CO_2 spectra were observed. These changes are more clearly seen in the CO_2 asymmetric stretch ν_3 band, shown in detail below. Spectra recorded between 105 K and the temperature of H_2O crystallization, ~165 K, did not show significant variations.

Additional measurements were performed on CO_2 sequentially deposited, both on amorphous and crystalline water ice. FTIR spectra were recorded as a function of the ice temperature for various CO_2 pressures, starting from 120 K and cooling until the first evidence of CO_2 was found in the spectra. The corresponding data were used for the estimation of desorption activation energies.

3. Results and discussion

3.1. TPD experiments

Figure 2 contains the most relevant results for our desorption experiments between 150 and 190 K. Due to the synchronization problems mentioned above, the abscissa values have to be taken with an uncertainty of ~5 K. The three upper panels correspond to the desorption of CO_2 from CO_2/amorphous water samples and the lowest one to the desorption of the host water layer. Water desorption, with a maximum at about 185–190 K,

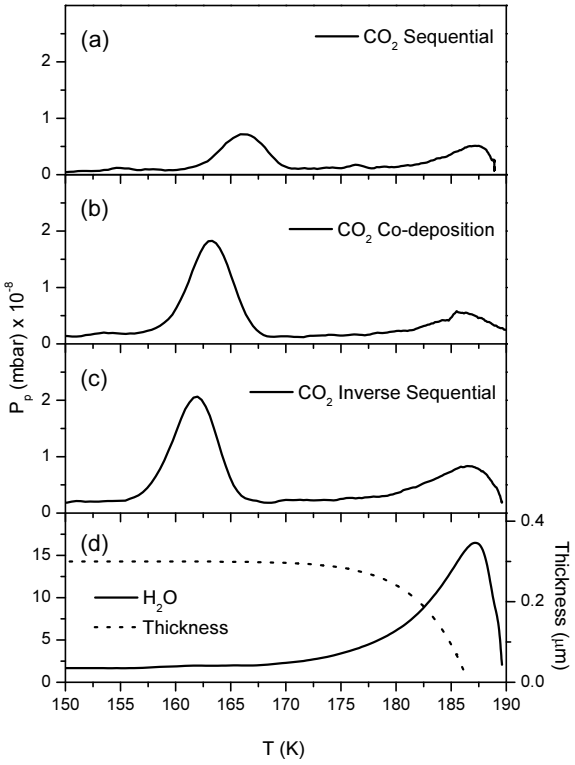

Fig. 2. TPD graphs for CO_2/H_2O ices deposited as specified (see text). The ordinate scale indicates QMS readings. *From top to bottom:* CO_2 curves for sequential deposition, co-deposition and inverse sequential deposition, and H_2O curve, plus estimation of sample thickness using Eqs. (1) and (2).

is similar in all cases and only one trace is shown for simplicity. A theoretical estimate of the desorption of the water film, based on a simple model, is also presented in the lowest panel (see below). In the case of CO_2/crystalline water all the CO_2 was desorbed at $T < 130$ K, and consequently it is not included in the figure. The signals corresponding to co-deposition and inverse sequential deposition are similar. Both show two maxima, one close to 165 K and a smaller one at about 185 K, coincident with the water peak. The location and intensity of the first desorption maximum are alike, the second maximum being somewhat larger in the inverse deposition experiment. Also two maxima at the same temperatures, within experimental uncertainty, albeit of lower intensity, are observed in the sequential deposition sample.

Several authors have studied the release of CO_2 and other gases from water ice (e.g. Bar-Nun et at. 1985; Hudson & Donn 1991; Collings et al. 2004). Although all of these investigations coincide with the observation of two desorption peaks for CO_2 in this temperature range, the actual temperature values measured for these peaks vary from one study to another, and furthermore the water maximum is found at different temperatures. The desorption of the water layer can be approximately modeled. Assuming zero-order kinetics, the time derivative of the film thickness as a function of temperature can be expressed as (Maté et al. 2003):

$$\frac{\mathrm{d}x}{\mathrm{d}t} = -\frac{a_0}{\rho}\exp\left(-\frac{E_\mathrm{d}}{RT}\right) \quad (1)$$

where x is the film thickness, ρ is the water density in the deposited film, E_d the desorption activation energy, a_0 the pre-exponential factor for zero-order kinetics, T the

surface temperature and R the gas constant. Equation (1) can be integrated over a given temperature interval by introducing the heating rate, $\upsilon_h = (dT/dt)$.

$$\int_{x_i}^{x_f} dx = -\int_{T_i}^{T_f} \frac{a_0}{\upsilon_h \rho} \exp\left(-\frac{E_d}{RT}\right) dT \quad (2)$$

where x_i and x_f are the initial and final thickness of the layer, and T_i and T_f the corresponding temperatures. Using Eq. (2) we have calculated the evolution of the water film thickness during our TPD experiments, with the result represented as a dotted line in the lower panel of Fig. 2. As can be seen, the calculated desorption corresponds well with the location of the measured TPD peak. The pre-exponential factor and the values of the desorption energy and water density used for the integration of Eq. (2) were: $a_0 = 2.8 \times 10^{30}$ molecules cm^{-2} s^{-1}; $E_d = 49.8$ kJ mol^{-1} and $\rho = 2.74 \times 10^{22}$ molecules cm^{-3}. These values were taken from Haynes et al. (1992) and Brown et al. (1996), and had already been used for estimates of water film thickness in a previous study by our group (Maté et al. 2003). As indicated above, the heating rate of our present experiments was $\upsilon_h = 0.3$ K s^{-1}. Given the uncertainty in the parameters of the model (Haynes et al. 1992; Brown et al. 1996) and the imprecision in the absolute temperature scale mentioned above, the good agreement between model and measurements could be a bit fortuitous, but in any case, the essential picture provided by Eqs. (1) and (2) seems to be correct.

The desorption of crystalline water films should take place at a slightly higher temperature, given the higher desorption energy of crystalline films reported in the literature (Sandford & Allamandola 1990; Sack & Baragiola 1993). However, the difference is small and is expected to lie within the experimental uncertainty of the present measurements. Similar observed temperature values and good agreement with the predictions of Eqs. (1) and (2) for the water desorption peak are reported by Bar-Nun et al. (1985) (observed maxima at ~180–200 K and predictions at 180–190 K), and Hudson & Donn (1991) (observed at ~175 K, predicted at 179 K). However, this value is measured at ~160 K by Collings et al. (2004), whereas the application of the simple model would yield a value of 179 K for the reported experimental conditions of that work. The reason for this discrepancy is not obvious. A density of $\rho \sim 2 \times 10^{22}$ molecules cm^{-3} was assumed in the model calculations for these experiments. This value should correspond (Brown et al. 1996) approximately to the conditions of Bar-Nun et al. (1985) and Hudson & Donn (1991), who deposited their samples at 20–30 K. The depositions of Collings et al. (2004) were performed at 10 K and for this temperature no values of ρ were reported (Brown et al. 1996). However, an appreciable change in density between 10 and 20 K would be needed to reconcile predictions and measurements.

Collings et al. also measured two CO_2 desorption peaks in this range. Our values are again shifted by about 20 K to higher temperatures, agreeing nonetheless with these authors in their separation and relative position to the water maximum.

The explanation given by Collings et al. (2004) for the two peak structures can be also applied to our experiments. The peak at ~165 K would thus correspond to the "volcano" desorption and the smaller peak at about 185 K is due to the co-desorption of the last trapped CO_2 molecules together with the water ice. The abrupt volcano desorption described by Smith et al. (1997) takes place through connected pathways formed in the water layer during the nucleation and growth of crystalline ice from ASW. The fact that our CO_2 volcano desorption peak is shifted by ~20 K toward temperatures higher than that of

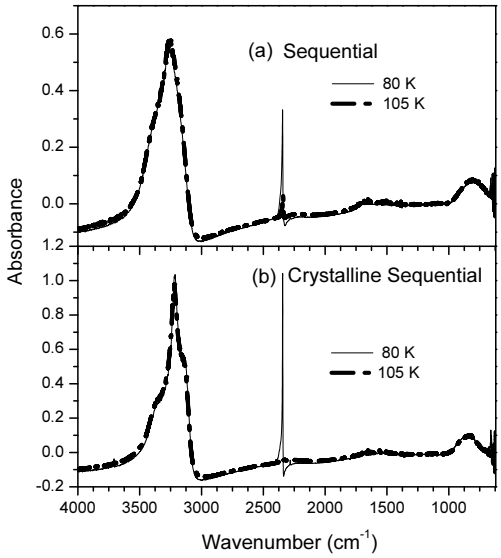

Fig. 3. IR spectra of H_2O and CO_2 mixtures in **a)** sequential and **b)** crystalline sequential deposition experiments, in the full mid-IR range recorded.

Collings et al. (2004) – precisely the same shift found between the peaks for the desorption of water – suggests that most of the water layer must crystallize before a significant amount of the trapped CO_2 is released. The crystallization rate of the water layer is determined by its thickness, density and heating rate. In accordance with the measurements of Collings et al., the volcano desorption peak in our experiments is stronger than that of co-desorption. The implications of this result for the interaction between the CO_2 and the ASW host layer are not yet clear. A comparison of the peak heights in the TPD records of the three different H_2O/CO_2 samples is also illustrative. The weaker desorption peaks found for the sequential deposition case show that a smaller amount of CO_2 is incorporated into the bulk water sample, as expected. Interestingly, no significant differences are observed between the desorption peaks of co-deposited samples and samples from inverse sequential deposition. For the samples of CO_2 deposited on crystalline water mentioned above, the absence of CO_2 desorption peaks for $T > 130$ K indicates that no CO_2 is incorporated into the crystalline water ice. A more detailed study of the desorption kinetics of CO_2 from water ice would be needed for full interpretation of these results.

3.2. FTIR spectra

Figure 3 presents IR spectra of sequentially deposited samples, initially at 80 K and after heating at 105 K. The upper frame shows the spectrum corresponding to sequential deposition and the lower panel to that of the crystalline sequential experiment. The water to CO_2 ratio is ~15:1, as in all the experiments described in this work. This figure is shown to highlight the following effects. The change between amorphous and crystalline water is reflected by the well-known narrowing of the O-H stretching region, 3000–3500 cm^{-1}, whereas the rest of the spectrum is practically unaffected. The consequence of the narrowing of the band is also an increase in the maximum absorbance of the peak (note the different absorbance scale in the two frames), keeping the overall band intensity unchanged. Interestingly, similar effects are observed on the ν_3 band of CO_2, which also becomes narrower (not easily seen in this compressed figure; see below where expanded traces of the spectra are shown

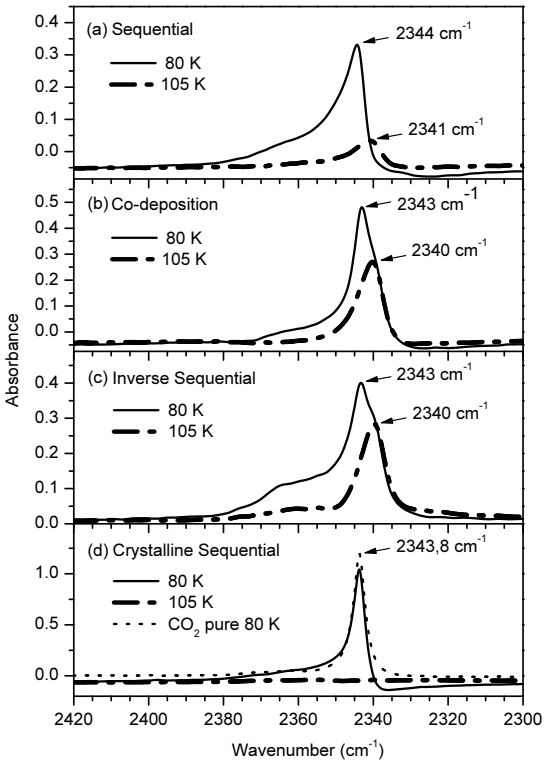

Fig. 4. IR spectra of samples of sequential deposition, co-deposition, inverse sequential deposition and crystalline sequential deposition, **a)** to **d)**, respectively. All spectra at 2 cm^{-1} resolution, and at temperatures indicated in each graph.

and discussed) and with a higher peak absorbance. Although at the deposition temperature of our experiments (80 K) CO_2 is expected to build up a crystalline solid, the fact that the substrate is crystalline rather than amorphous water induces an apparently higher degree of crystallinity in the CO_2 structure (Albella 2003). Finally, the dashed trace of the 105 K spectrum in the lower frame indicates that all CO_2 has been desorbed at this temperature.

As mentioned above, the expanded region of the ν_3 band of CO_2 allows a better observation of spectral changes induced by the heating of the samples, as no signifi cant variations are detected in the spectra of water in this spectral zone. Figure 4 shows transmission IR spectra of the mixtures of water and CO_2 in this region. The samples were deposited at 80 K, and spectra were recorded at this temperature. They were then heated and kept at 105 K until no variation was detected in the quadrupole spectrometer, indicating that gas release at this temperature was completed. This happened systematically in less than 2 minutes. Spectra were subsequently registered. Note that the intensity scale takes fairly large values in absorbance units, which indicates that strong absorptions of CO_2 are taking place in all samples. The top panel corresponds to sequential deposition; it can be seen that after heating, a weaker band appears at ~2341 cm^{-1}, i.e. shifted by ~3 cm^{-1} to lower wavenumber. The next panel represents a co-deposited sample. The spectrum at 80 K shows a maximum at 2343 cm^{-1}, with a shoulder on the low-frequency slope of the main band; after heating, this shoulder is revealed as a clear band peaking at ~2340 cm^{-1}. Panel (c) displays the spectra corresponding to the inverse sequential deposition experiment, and presents a very similar pattern to that of co-deposited samples, although in this case an ASW layer has grown on top of CO_2 ice. Finally, the bottom panel shows the spectra of CO_2 sequentially deposited on crystalline water. After heating, all CO_2 is desorbed from the sample. The spectrum of pure CO_2 is also displayed for comparison. The main difference between the spectrum of pure CO_2 and that deposited at 80 K on crystalline water is the asymmetry of the ν_3 band of the latter, which is also a feature of the 80 K spectrum of the sequential sample. The global consideration of the previous results indicates that there are two different mechanisms of interaction of CO_2 and water, leading to two slightly different CO_2 structures. The most relevant one at 80 K is characterized by a strong peak at ~2343–2344 cm^{-1}, close to that of pure CO_2. In the second CO_2 structure the main peak is shifted to a lower frequency, at ~2340 cm^{-1}. This shifting must be due to the interaction of CO_2 with surrounding water, resulting in a slight weakening of the C-O bond, the lower frequency indicating a reduced value of the effective stretching force constant. Thus, to avoid lexical repetitions we may term these two structures CO_2-ext and CO_2-int, for external and internal, respectively, meaning by external that the interaction with water is quite weak as it would be if CO_2 were superfi cially adsorbed, for instance, and by internal the situation taking place when CO_2 molecules enter the pores of ASW. These two possible mechanisms have been discussed by Kumi et al. (2006), and we will emphasize here only those aspects that supply new evidence for this problem.

When CO_2 is sequentially deposited at 80 K (panel a of Fig. 4), it forms a structure with very little interaction with the host surface, as indicated by the position of the ν_3 band, and apparently without entering the amorphous water structure, given the absence of any low-frequency shoulder on that band. This CO_2 layer can be very thick, giving a strong infrared absorption signal. After heating, the CO_2-ext is fully desorbed, but a small fraction is kept inside the ASW, as shown by the weak spectral absorption peak at ~2340 cm^{-1} at 105 K.

In co-deposition experiments, panel b, the two CO_2 structures coexist at 80 K. The main band has a peak at the frequency of the CO_2-ext structure and a small shoulder at that of the CO_2-int form. When the sample is heated, one band only at the CO_2-int frequency remains, stronger than the corresponding shoulder observed at 80 K. This therefore indicates, on one hand, that no CO_2- ext is kept, and on the other that apparently a fraction penetrates the bulk amorphous water, or adopts the CO_2-int structure.

Panel c in Fig. 4 shows the spectra recorded after inverse sequential deposition. The pattern is similar to that of co-deposition, with the strongest peak at 80 K corresponding to CO_2-ext, and a shoulder at the vibrational frequency of the CO_2-int structure. After heating, only CO_2-int remains. When water is deposited on top of a CO_2 ice, part of the CO_2 breaks its own crystalline structure and diffuses into the amorphous water layer above. The pressure that the ASW layer exerts on the CO_2 ice could be high enough to enable this effect, which is not observed when CO_2 is deposited on top of ASW in direct sequential deposition experiments. Kumi et al. (2006) performed a series of measurements in which CO_2 is " sandwiched" between two amorphous water fi lms, and their results also prove that the pressure of the ASW layer on top of the CO_2 structure increases the formation of CO_2-int.

Since the spectra recorded at 140 K (not shown here) do not present any signifi cant variations with respect to those taken at 105 K, we may conclude that in all cases, the CO_2 diffused in the interior of ASW remains included until the water crystallization takes place, at ~165 K.

Panel d of Fig. 4 displays the spectra corresponding to CO_2 deposition on crystalline water. At 80 K the CO_2 is retained

on the surface but, as indicated in the previous comments on the TPD measurements, this layer of CO_2 desorbs completely upon heating and is unable to penetrate the crystalline ice structure. Kumi et al. describe this situation in terms of closing of the pores existing in amorphous water during the crystallization. Comparison of panels a and d reveals the different CO_2 adsorption mechanism at 80 K for ASW and for crystalline water, as a consequence of the different nature of the corresponding water surfaces. The contour of the CO_2 ν_3 band is sharper in the crystalline water experiment, and is in fact closer to that of a pure CO_2 sample grown directly on the substrate, shown also in panel d. It can be inferred from this that CO_2 adopts a more homogeneous structure when grown on top of a crystalline surface. It is also worth observing that the bandshape of the spectra of CO_2 adsorbed both on the amorphous and crystalline water surfaces is clearly asymmetrical, with an intensity drop on the low-frequency side, whereas in the spectrum of pure CO_2 ice this band is more symmetrical. This effect could be interpreted in terms of the interaction of CO_2 with the surface of water, which induces a modified structure for the first CO_2 layer in contact with the water surface (Ovchinnikov & Wight 1993).

The P–polarized transmission spectra presented by Kumi et al. were obtained at low exposure pressure, namely 4×10^{-8} Torr for CO_2, and the films formed under these conditions are more favorable for the observation of weak effects, such as the appearance of a thin peak at 2379 cm^{-1} in a sequential deposition experiment at 90 K. This peak is present as a weak and broader feature shifted to ~2370 cm^{-1} in all our spectra at 80 K, and has been interpreted as the longitudinal mode coupled to the transverse mode at ~2343 cm^{-1} (Ovchinnikov & Wight 1993). Kumi et al. recorded spectra of the very weak amount of CO_2 that remains embedded into their thin ASW films upon heating at 105 K, which we have called here CO_2-int. The peak absorption of the corresponding ν_3 band reaches a maximum of ~0.02 for a water film of ~65 layers, becoming saturated, and not increasing at higher doses of CO_2 at 90 K. This weak peak is also observed in our sequential deposition spectrum at 105 K, corresponding to experiments similar to those of Kumi et al., but performed on thicker water layers. In contrast, our results for co-deposition and inverse sequential deposition allow a much stronger absorption to be recorded for the ν_3 band of the CO_2-int structure, with a peak absorbance of ~0.25 in panels b and c. This proves that for higher water/CO_2 ratios in the co-deposition or in the inverse sequential deposition scheme, the intensity of that peak is increased, indicating a larger amount of CO_2 introduced within ASW, in agreement with the conclusions of Kumi et al., that the higher water to CO_2 ratio allows more CO_2 to occupy sites or vacancies inside the ASW structure.

The region corresponding to the same band for $^{13}CO_2$ provides clearer evidence of the co-existence of the two CO_2 structures, as the shift between them is larger for this isotope. Figure 5 presents zoomed-in spectra in the ν_3 region of $^{13}CO_2$, ~2280 cm^{-1}, recorded for sequential deposition (top) and co-deposition (bottom). At 80 K (solid line), only one peak is seen in the first case, corresponding to $^{13}CO_2$-ext, and two peaks in the second, arising from both $^{13}CO_2$-ext and $^{13}CO_2$-int, with a displacement of ~7 cm^{-1}. At 105 K the CO_2-ext trace has almost completely vanished, and the CO_2-int spectrum is detected by a very weak peak in the co-deposition experiment only (dotted-dashed line).

We can make use of a simple molecular model based on Wilson's GF matrix scheme (Wilson et al. 1955) to gain insight into the properties of the ν_3 asymmetric stretching mode. Both the G and F matrices are one-dimensional for this vibration, with

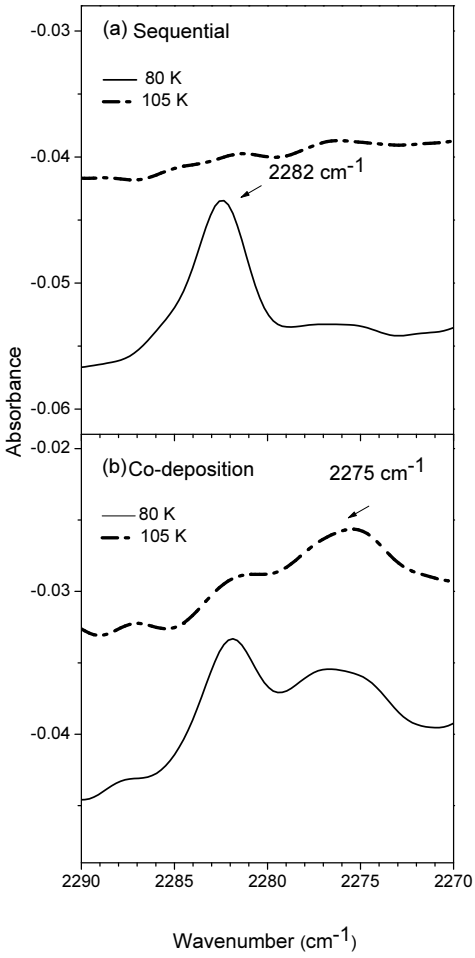

Fig. 5. IR spectra of the ν_3 band of $^{13}CO_2$ for **a)** sequential and **b)** co-deposited samples, at the temperatures indicated.

matrix elements $g = 2\mu_C+\mu_O$ and $f = f_{st}-f'_{st-st}$ respectively. The μ_x are the reciprocal masses of the corresponding atoms (x = O or C), and f_{st} and f'_{st-st} represent the force constants for the stretching of the C-O bond and for the interaction between both stretchings, respectively. The frequency of the ν_3 mode is therefore given by the following equation (Herzberg 1991):

$$\nu = \frac{1}{2\pi c}\sqrt{\left(f_{st} - f'_{st-st}\right)(2\mu_c + \mu_0)}. \quad (3)$$

A frequency shift of ~4 cm^{-1} in the wavenumber of this vibration, from ~2344 to ~2340 cm^{-1}, would therefore correspond to a weakening of the f_{st} force constant of the $^{12}CO_2$-int structure with respect to that of $^{12}CO_2$-ext by a factor of $f_{st}^{int}/f_{st}^{ext}$ ~ 0.997, or 0.3 %. The effect of the surrounding water molecules on the CO_2-int structure can be estimated to be of that magnitude. Note also that in this simple model the C-O bond length is not relevant. For the ^{13}C vibration, where the shift is larger, ~7 cm^{-1} from ~2282 to ~2275 cm^{-1}, the weakening effect is also slightly more marked, $f_{st}^{int}/f_{st}^{ext}$ ~ 0.994. This is due to the fact that the $^{13}CO_2$-ext vibration does not strictly follow the isotopic mass ratio expected from Eq. (3) (predicted at at ~2277 cm^{-1} and observed at ~2282 cm^{-1}), whereas the vibration of the $^{13}CO_2$-int structure complies more closely with it (predicted at ~2273 cm^{-1}, observed at ~2275 cm^{-1}).

In a very recent investigation, Chaban et al (2007) calculated the harmonic and anharmonic vibrational frequencies of clusters of CO_2 and a number of water molecules by ab initio methods.

Table 1. Ice temperatures for which CO_2 adsorption ceases as a function of CO_2 pressure.

CO_2-amorphous water ice		
T-ice (K)	P-CO_2 (mbar)	E_d (kJ mol^{-1})
90	7.0e−6	20.8
92	1.4e−5	20.7
98	1.0e−4	20.5
CO_2-crystalline water ice		
T-ice (K)	P-CO_2 (mbar)	E_d (kJ mol^{-1})
90	2.3e−5	19.9
93	4.8e−5	20.0
95	1.0e−4	19.8

They found a shift towards higher frequencies when one or two water molecules are added to pure CO_2, in agreement with some observations on planetary satellites. The structure of the clusters studied by Chaban et al (2007) is probably very different to that of the ice systems investigated in this paper, and thus our respective results cannot be directly compared.

3.3. Desorption energies

Energies of desorption are often derived from TPD measurements. However, this procedure is problematic in the present case. In addition to the already mentioned experimental difficulties for the observation of neat desorption peaks below ∼110 K with the available cryostat (Sect. 2), the CO_2 desorption energies from CO_2 surfaces and from H_2O surfaces are similar (Sandford & Allamandola 1990). Thus, even if it were possible to measure the CO_2-H_2O (monolayer) desorption it would be very difficult to distinguish it from the CO_2-CO_2 desorption. Therefore, rather than using TPD measurements we have employed a method analogous to that of Sandford and Allamadola (1990) based on the observation of the sticking of CO_2 to the ice surfaces as a function of CO_2 pressure and ice temperature. In our experiments sequential deposition was performed on the surfaces of pure amorphous and crystalline water ice and the amount of deposited CO_2 was monitored with FTIR measurements. For a given CO_2 pressure, the initial ice temperature was cooled from 120 K down in 2 K intervals until some evidence of CO_2 deposition was observed in the FTIR spectra. The results of these measurements, which were found to be very repetitive, are listed in Table 1 together with the desorption energies obtained from them.

For the derivation of the E_d values it was assumed that CO_2 deposition ceases when the average residence time of the molecules on the surface, t_s, is equal to the time during which the ice surface is hit by a number of CO_2 molecules equivalent to one monolayer coverage, t_m. It was further assumed that the desorption of CO_2 from ice surfaces can be described by the models of Langmuir (1916) and Frenkel (1924) in which t_s is given by

$$t_s = t_0 \exp(E_d/RT) \quad (4)$$

where E_d is the activation energy for desorption and t_0 the period of oscillation of the molecule at the surface. The value of t_m was obtained as

$$t_m = \frac{n_s}{\varphi} \quad (5)$$

where n_s is the CO_2 monolayer surface density and φ is the flow of molecules to the surface for a given CO_2 pressure. For the estimation of n_s, a mean seat area of 15.5 Å^2 (Sandford & Allamandola 1990; Barret & Meyer 1965) was assumed and the molecular flow to the surface was calculated from gas kinetic theory as: $\varphi = (1/4)n\langle v\rangle$, where n is the molecular density for a given CO_2 pressure and $\langle v\rangle$ is the average molecular velocity at the corresponding gas temperature. Setting $t_s = t_m$ in Eq. (4), and substituting t_0 for its associated oscillation frequency, $\nu_0 = 1/t_0$, the activation energy for desorption can be expressed as

$$E_d = RT\ln(\nu_0 t_m). \quad (6)$$

We have taken $\nu_0 = 2.9 \times 10^{12}$ s^{-1} for the frequency of oscillation; this is the value used by Sandford & Allamandola (1990) and corresponds to an average of librational modes of CO_2. The average values of the desorption energy obtained from the present experiments are $E_d = 20.7 \pm 2$ kJ mol^{-1} for the adsorption of CO_2 on amorphous ice, and $E_d = 19.9 \pm 2$ kJ mol^{-1} for the adsorption of CO_2 on crystalline ice. The E_d for crystalline ice is slightly lower (0.8 kJ mol^{-1}) that that for amorphous ice, but the difference is small in comparison with the estimated uncertainties. Note that the uncertainty is mostly due to the assumptions made in the calculation of the $\nu_0 t_m$ product.

The E_d value for amorphous ice obtained in the present experiments is ∼15% lower than that of Sandford & Allamadola (1990) ($E_d = 23.7 \pm 1.7$ kJ mol^{-1}) which was obtained with a similar procedure. The discrepancy is not too large taking into account the respective uncertainties. There are also some differences in the experimental details. In the present study CO_2 was deposited on pure ice surfaces whereas Sandford and Allamandola deposited CO_2/H_2O mixtures. In a recent article Anderson et al. (2004) reported an activation energy $E_d = 21.2 \pm 1.9$ kJ mol^{-1} for the desorption of CO_2 from crystalline ice. This value, obtained from time-resolved molecular beam measurements, is slightly larger (∼6.5%) than ours, but both lie within the mutual experimental uncertainty. The agreement is reassuring taking into account the different experimental methods used. The molecular beam experiments of Anderson et al. (2004) also show that the interaction of CO_2 with amorphous ice is more complex than that with crystalline ice. This observation is in agreement with the results of the present study discussed above.

4. Conclusions

The main contributions of this work are related to the fact that the systems under consideration are studied simultaneously using two different techniques, with results that complement each other. In addition, we have dealt with four different types of samples corresponding to four different deposition schemes, at temperatures between 80 and 190 K, whereas in previous studies a more reduced set of data was employed. In particular, our water layers deposited at 80 K are expected to have a higher density than those of the previous TPD studies on the H_2O/CO_2 system. Collings et al. (2004) worked with sequentially deposited and co-deposited samples formed at very low temperature (8–10 K), and heated at a slower pace of 0.08 K s^{-1}. Their TPD experiments are carried out for concentrations of about 5% of the guest molecule in water, fairly similar to our H_2O/CO_2 ratio of ∼15/1. The reasons for the temperature discrepancies between the results of Collings et al. and those of the present work and of other authors (Bar-Nun et al. 1985; Hudson & Donn 1991) are not entirely clear but might be related to the different density of the ices formed and to the different heating rate of the desorption experiences. It is conceivable that a higher porosity, as expected from a lower temperature deposition, and a slower

heating pace, which may allow more pores to open per unit of time, permit embedded CO_2 to escape at lower temperatures in the experiment of Collings et al. (2004). More systematic studies of desorption as a function of deposition conditions would certainly be worthwile.

We have also carried out experiments at smaller CO_2 concentrations, but the results simply change proportionally to the relative concentration of the species, and therefore are not commented on in this paper.

The experiments of Kumi et al. (2006) were carried out on sequentially deposited samples at lower exposure pressures, but the general conclusions are similar to those of the present investigation. The new evidence put forward in this study correspond to co-deposition and crystalline deposition experiments. Our co-deposition results provide increased data on the formation of a second CO_2 structure associated with ASW. Also, we present new evidence in the region of the ν_3 band of the ^{13}C isotopomer. The vibration of $^{13}CO_2$-ext, at 2282 cm^{-1}, is seen only at 80 K, just as in sequential deposition traces, but the corresponding vibration of $^{13}CO_2$-int, although very weak, can be detected with a shift of $\sim$7 cm^{-1} after heating to 105 K.

We also provide here an estimate of the activation energies for the desorption of CO_2 from surfaces of amorphous (E_d = 20.7 ± 2 kJ mol^{-1}) and crystalline water ice (E_d = 19.9 ± 2 kJ mol^{-1}), which are in reasonably good agreement with the previous results by Sandford & Allamandola (1990) and by Anderson et al. (2004) respectively.

Sandford & Allamandola (1990) worked with co-deposited samples of quite different concentrations, including also samples with methanol. They observed large changes in wavenumber and width of the CO_2 vibrations, on heating from 10 to 150 K, and associated these changes with the relative concentrations of CO_2 and water. Our results seem to show two slightly different CO_2 structures, which prevail depending not only on the temperature but also on the deposition method, even for similar temperatures. We have also shown that CO_2 can become attached to crystalline water ice at 80 K, although it completely escapes on heating to 105 K. These findings have astronomical relevance, especially for icy bodies of the Solar System. For example, for cometary nuclei, the two different varieties of CO_2-water association might have some influence in their thermophysical evolution. The spectroscopic differences due to the deposition method are also important for the characterization of the formation and evolution of cometary nuclei, and especially, of transneptunian objects, which have been found to contain both crystalline and amorphous water ices.

Acknowledgements. This work has been funded by the Spanish Ministry of Education, project FIS2004–00456. Part of this work has also been supported by the Spanish National Research Council (CSIC) under project HIELOCRIS-PIF2005. PJG and OG acknowledge financial support from the Spanish Ministerio de Educación y Ciencia, programs "Ramón y Cajal" and "Juan de la Cierva", respectively. We would like to thank the Editor and the referee for helpful comments on the manuscript which have prompted some additions to the original results.

References

Albella, J. M. 2003, Láminas Delgadas y Recubrimientos. Preparación, propiedades y aplicaciones, Biblioteca de Ciencias, CSIC
Andersson, P. U., Någård, M. B., Witt, G., et al. 2004, J. Phys. Chem. A, 108, 4627
Baker, M. B. 1997, Science, 276, 1072
Bar-Nun, A., & Laufer, D. 2003, Icarus, 161, 157
Bar-Nun, A., Herman, G., Laufer, D., et al. 1985, Icarus, 63, 317
Barrett, C. S., & Mayer, L. 1965, J. Chem. Phys. 43, 3502
Bernstein, M. P., Cruikshank, D. P., & Sanford, S. A. 2005, Icarus, 179, 527
Bernstein, M. P., Cruikshank, D. P., & Sanford, S. A. 2006, Icarus, 181, 302
Boogert, A. C. A., & Ehrenfreund, P. 2004, Interstellar Ices, ed. A. N. Witt, G. C. Clayton, & B. T. Draine, ASP Conf. Ser., 309, 547
Brown, D. E., George, S. M., Huang, C., et al. 1996, J. Phys. Chem., 100, 4988
Buratti, B. J., Cruikshank, D. P., Brown, R. H., et al. 2005, ApJ, 622, L149
Carrasco, E., Castillo, J. M., Escribano, R., et al. 2002, Rev. Sci. Inst., 73, 3469
Chaban, G. M., Bernstein, M. & Cruikshank, D. P. 2007, Icarus, 187, 592
Collings, M. P., Anderson, M. A., Chen, R., et al. 2004, MNRAS, 354, 1133
Crovisier, J. 2006, Mol. Phys. 104, 2737
Dartois, E. 2005, Space Sci. Rev., 119, 293
Ehrenfreund, P., Boogert, A. C. A., Gerakines, P. A., et al. 1997, A&A, 328, 649
Ehrenfreund, P., Kerkhof, O., Schutte, W. A., et al. 1999, A&A, 350, 240
Ehrenfreund, P., Fraser, H. J., Blum, J., et al. 2003, Planet. Space Sci., 51, 473
Escribano, R., Couceiro, M., Gómez, P. C., et al. 2003, J. Phys. Chem. A, 107, 651
Frenkel, Z. 1924, Z. Phys. 26, 117
Gerakines, P. A., Bray, J. J., Davis, A., et al. 2005, ApJ, 620, 1140
Grundy, W. M., & Schmitt, B. 1998, J. Geoph. Res., 103, 25809
Haynes, D. R., Tro, N. J., & George, S. M. 1992, J. Phys. Chem., 96, 8502
Herzberg, G. 1991, Infrared and Raman Spectra of Polyatomic Molecules, Vol. II, Molecular Spectra and Molecular Structure, Krieger, Florida
Hudson, R. L., & Donn, B. 1991, Icarus, 94, 326
Hung, H.-M, Malinowski, A., & Martin, S. T. 2003, J. Phys. Chem. A, 107, 1296
Kumi, G., Malyk, S., Hawkins, S., et al. 2006, J. Phys. Chem. A, 110, 2097
Langmuir, I. 1916, Phys. Rev., 8, 149
Léger, A., Gauthier, S., Défourneau, D., et al 1983, A&A, 117, 164
Maté, B., Medialdea, A., Moreno, M. A., et al. 2003, J. Phys. Chem. B, 107, 11098
Maté, B., Ortega, I. K., Moreno, M. A., et al. 2006, J. Phys. Chem. B, 110, 7396
Meech, K., & Svoren, J. 2003, Using cometary activity to trace the physical and chemical evolution of cometary nuclei, In Comets II, ed. Festou, Keller & Weaver (University of Arizona Press), 317
Moore, M. H., & Hudson, R. L. 1993, ApJ, 401, 353
Moore, M. H., Hudson, R. L., Gerakines, P. A. 2001, Spectrochim. Acta Part A, 57, 843
Notesco, G., Bar-Nun, A., & Owen, T. 2003, Icarus, 162, 183
Ovchinnikov, M. A., & Wight, C. A. 1993, J. Chem. Phys., 99, 3374
Quirico, E., Schmitt, B., Bini, R., et al 1996, Planet. Space Sci., 44, 973
Sack N. J., & Baragiola, R. A 1993, Phys. Rev B, 48, 9973
Sandford, S. A., & Allamandola, L. J. 1990, ApJ, 355, 357
Satorre, M. A., Palumbo, M. E., & Strazzulla, G. 2001, J. Geophys. Res., 106. 33363
Schmitt, B., Greenberg, J. M., & Grim, R. J. A. 1989, ApJ, 340, L33
Smith R. S., Huang, C., Wong, E. J. L., et al. 1997, Phys. Rev. Lett., 79, 909
Tolbert, M. A., & Toon, A. O. B. 2001, Science, 292, 61
Van Dishoeck, E. F. 2004, Ann. Rev. A&A, 42, 119
Van Broekhizen, F. A., Groot, I. M. N., Fraser, H. J., et al. 2006, A&A, 451, 723
Viti, S., Collings, M. P., Dever, J. W., et al. 2004, MNRAS, 354, 1141
Wilson, E. B., Decius, J. C., & Cross, P. C. 1955, Molecular Vibrations (N. Y.: Dover Publications)